

# **Ab initio model potential study of pressure effects on $\text{K}_2\text{NaGaF}_6\text{:Cr}^{3+}$**

Luis Seijo and Zoila Barandiarán

*Departamento de Química Física Aplicada, C-14, Universidad Autónoma de Madrid, 28049 Madrid, Spain*

Lars G. M. Pettersson

*Institute of Theoretical Physics, University of Stockholm Vanadisvägen 9, S-113 46 Stockholm, Sweden*

(Received 2 November 1992; accepted 16 November 1992)

In this paper we present the results of an *ab initio* study of the pressure effects on the  $^4A_{2g}$  ground state and the  $^4T_{2g}$  and  $^2E_g$  excited states of  $\text{Cr}^{3+}$ -doped  $\text{K}_2\text{NaGaF}_6$ . Complete active space SCF (CASSCF) and averaged coupled-pair functional (ACPF) calculations are performed on a  $\text{CrF}_6^{3-}$  cluster embedded in an *ab initio* model potential (AIMP) representation of the  $\text{K}_2\text{NaGaF}_6$  lattice at ambient and high pressure. The results are in close agreement with the experimentally measured pressure shifts of vibrational frequencies and emission spectra, which demonstrates the ability of the *ab initio* embedding model potential method to accurately model hydrostatic pressure experiments in this type of defect crystals. It is also shown that if only the standard Madelung embedding potential is used, none of the observed effects of pressure are reproduced.

## **I. INTRODUCTION**

Halide elpasolite crystals ( $\text{A}_2\text{BMX}_6$ , where A and B are monovalent cations, M is a trivalent cation, and X is a halogen anion), doped with  $\text{Cr}^{3+}$  have been the subjects of spectroscopic investigations at both ambient and elevated pressures due to their potentiality as tunable solid-state laser materials.<sup>1–11</sup> In these compounds the substitutional  $\text{Cr}^{3+}$  impurity is accommodated at a rigorously octahedral site without charge compensation. At ambient pressure they have been shown to exhibit low-crystal-field behavior characterized by broad-band  $^4T_{2g} \rightarrow ^4A_{2g}$  fluorescence, in contrast with the narrow-band  $^2E_g \rightarrow ^4A_{2g}$  phosphorescence typical of high-field complexes.<sup>1,6,7</sup>

In these materials, the photoluminescence has been shown to be very environment dependent in two different ways: (i) The thermal quenching of fluorescence at ambient pressure is found to be strongly host dependent,<sup>7,8</sup> and (ii) the pressure dependence of photoluminescence in  $\text{K}_2\text{NaGaF}_6\text{:Cr}^{3+}$  shows the possibility of a pressure-induced transition from low-field to high-field behavior.<sup>6</sup> In effect, as pressure is increased from 0 to 61 kbar, a blueshift of the broad  $^4T_{2g} \rightarrow ^4A_{2g}$  band is observed while a highly structured  $^2E_g \rightarrow ^4A_{2g}$  phosphorescence band develops. This evolution is interpreted as the consequence of different pressure effects on the excited states involved: While the  $10Dq$  state  $^4T_{2g}$  is shifted to higher energy values relative to the ground state, as pressure is increased, the intraconfigurational  $^2E_g$  state remains virtually insensitive to pressure.<sup>6</sup> The vibrational frequencies have also been found to be affected by hydrostatic pressure.<sup>6,9,10</sup>

From the theoretical point of view, modeling the ground and excited state electronic structures of a defect system, such as  $\text{K}_2\text{NaGaF}_6\text{:Cr}^{3+}$ , through standard *ab initio* quantum chemical methods still remains a major challenge, as it has been recently pointed out by Pierloot and Vanquickenborne<sup>12</sup> in a detailed investigation of the correlation effects on the (absorption) ligand field spectrum of the isolated hexafluorochromate (III) anion. The difficulties increase when the characteristics of the potential en-

ergy surfaces of ground and excited states that are relevant to the laser activity (i.e., equilibrium geometries, crossing points, curvatures), have to be calculated in order to carry out detailed studies of absorption/emission spectra, possible quenching mechanisms, excited state absorption spectra, etc., because these properties depend not only on intracenter correlation effects, but also on the environmental effects due to the interactions with the crystal components beyond the immediate ligands.

Yet, it is very desirable to be able to conduct reliable and accurate *ab initio* calculations on this kind of system and properties, since the information attainable from the calculations (i.e., the topology of the energy surfaces) is complementary to that obtained by the use of the different available experimental techniques.

In this line, and as a result of a search for accurate representations of the crystalline environment of a given cluster, the *ab initio* environment model potential method (AIEMP)<sup>13,14</sup> has been proposed and used as the solid-state replica of the *ab initio* molecular core model potentials,<sup>15</sup> with the ability of bringing into cluster calculations quantum mechanical interactions with the crystalline environment (exchange, orthogonality, quasirelativistic effects), which enable the accurate calculation of local geometries and local-geometry dependent properties (i.e., emission transitions, Jahn–Teller distortions, etc.) at a cost only slightly higher than a Madelung representation of the lattice.

Since the reproduction of the subtle differential environmental effects corresponding to high pressure experiments such as performed by Dolan *et al.*<sup>6</sup> poses a major challenge to any embedding theory, we have conducted an *ab initio* study of the  $^4A_{2g}$  ground state and the  $^4T_{2g}$  and  $^2E_g$  excited states of the  $\text{CrF}_6^{3-}$  cluster embedded in an AIEMP representation of the  $\text{K}_2\text{NaGaF}_6$  lattice, both at ambient pressure and at 61 kbar. The overall close agreement of the calculated and experimental pressure shifts shows the ability of the *ab initio* embedding model potential method to accurately model hydrostatic pressure experiments in this type of defect crystals.

## II. METHOD

The *ab initio* environment model potential method used to perform the embedded cluster calculations at different pressures has been presented in Refs. 13 and 14; here we only summarize its main features. The method enables the application of the group function theory developed by McWeeny<sup>16</sup> and by Huzinaga<sup>17</sup> to the calculation of local properties of imperfect crystals like  $K_2NaGaF_6:Cr^{3+}$ . Its application to this particular system is based upon the assumption that the *local properties* of the embedded  $CrF_6^{3-}$  unit, i.e., its structure and ligand-field electronic transitions, should not be affected by cluster-lattice correlation effects, which are not included in the formalism, but only by intracluster correlation effects and nondynamical quantum mechanical interactions with the environment such as long/short-range Coulomb, exchange and orthogonality interactions. This is expressed by the following antisymmetric product wave function which is expected to represent a good approximation of the imperfect crystal local electronic states:

$$\Psi^{crys} \simeq M\hat{A}[\Phi_{CrF_6^{3-}} \Phi_{K^+} \dots \Phi_{Na^+} \dots \Phi_{Ga^{3+}} \dots \Phi_{F^-} \dots] \quad (1)$$

with the corresponding total energy expression

$$E^{crys} \simeq E_{CrF_6^{3-}} + E_{CrF_6^{3-}-env} + E^{env} \quad (2)$$

which takes this form when the embedded group functions are strongly orthogonal.<sup>16</sup>

In fact, the embedded-group wave functions  $\Phi_{CrF_6^{3-}}$  and  $[\Phi_{K^+} \dots \Phi_{Na^+} \dots]$  can be any suitable mono- or multiconfigurational expansion which can be obtained variationally and iteratively until all of them converge to some self-consistent (fully polarized) solution.<sup>16,18</sup> Alternatively, they can be obtained all at once in a single iteration where, in particular, the cluster group function is calculated (variationally) as embedded in a set of *frozen* environment group functions located at their crystallographic sites, resulting in the *frozen environment* approximation which constitutes the extended system analogy to the molecular frozen core approximation. The frozen environment approximation is expected to give the environmental effects on local properties, such as those studied in the present work, of the embedded cluster.

A direct application of this approach would require the calculation of Coulomb and exchange integrals between the cluster and the various environment group functions, which have been collected in the term  $E_{CrF_6^{3-}-env}$ , and further approximations are thus required. These approximations are based on the ideas of the *ab initio* core model potential method,<sup>15</sup> so that complete-ion model potentials representing the true environment potentials acting on the cluster are obtained directly from the group wave functions  $(\Phi_{K^+}, \Phi_{Na^+}, \Phi_{Ga^{3+}}, \Phi_{F^-})$  without the use of any parametrization procedure. The embedding model potentials, which are straightforwardly added to the one-electron cluster Hamiltonian, explicitly include the long-range and short-range Coulomb interactions, the quantum exchange interactions and the quantum orthogonality interactions:

$$V_{lr-Coul}^{I,MP}(i) + V_{sr-Coul}^{I,MP}(i) + V_{exch}^{I,MP}(i) + Proj^I(i) \quad (3)$$

where  $I=K^+, Na^+, Ga^{3+}, F^-$ .

In the following we present the details of the frozen environment cluster calculations performed: construction of the environment group functions, embedding potentials and the expansions used for the defect cluster wave functions.

### A. The environment: Ambient pressure embedding potential

Owing to the ionic character of the host  $K_2NaGaF_6$  crystal, acceptable descriptions of the external  $\Phi^I$  ( $I=K^+, Na^+, Ga^{3+}, F^-$ ) group functions, suitable to generate the *ab initio* (frozen) embedding model potentials, have been obtained from closed-shell monoconfigurational self-consistent embedded ion calculations<sup>19</sup> performed on the perfect host crystal structure at ambient pressure ( $O_h-F_{m3m}$ ,  $a_0=8.246$  Å,<sup>20</sup>  $x_F=0.235$   $a_0$ ,<sup>21</sup> where  $a_0$  is the lattice parameter). The basis sets used for these embedded-ion calculations are the uncontracted  $K^+$  (9/6),  $Na^+$  (6/3),  $Ga^{3+}$  (9/6/4), and  $F^-$  (6/4) sets; the exponents were obtained from maximum overlap fittings to the orbitals from numerical HF isolated ion calculations. The final outcome of these preparatory calculations are the self-consistent  $\Phi^I$  ( $I=K^+, Na^+, Ga^{3+}, F^-$ ) group functions and the corresponding total-ion *ab initio* model potentials. The ambient pressure AIEMP for the  $CrF_6^{3-}$  defect cluster is now built up by adding the contributions of all ions located within the cube (centered at the impurity site) whose edge is 4  $a_0$ . Of these ions, the first 82 neighbors are represented by the total ion *ab initio* embedding model potentials which we have just described; the remaining as point charges bearing the ionic charges corresponding to a completely ionic crystal in all cases except for the frontier ions for which Evjen's fractional charges are used.<sup>22</sup> The *ab initio* embedding model potential corresponding to ambient pressure ( $a_0=8.246$  Å) will be referred to as AIEMP(0).

### B. The environment: High pressure embedding potential

The high pressure representation of the environment is readily obtained following the same steps as described above for ambient pressure, but using the host crystal structure corresponding to the high pressure data instead.<sup>23</sup> This means that either the isothermal bulk modulus or the variation of the lattice constant with pressure,  $a_0(P)$ , is required. In this respect, as far as we know, the isothermal bulk modulus has not been measured for the host  $K_2NaGaF_6$ . Instead, the percent reduction of the lattice parameter as a function of hydrostatic pressure has been estimated by Sinkovits and Bartram<sup>11</sup> from empirically parametrized lattice dynamics simulations. According to their plots of hydrostatic pressure vs  $\Delta a_0/a_0$  (Fig. 2 of Ref. 11), a reduction by about 3% would correspond to an applied pressure of 60 kbar. Consequently, we have taken as the new value for the lattice constant  $a_0(60 \text{ kbar})=8.000$  Å, in order to model the high pressure experiments performed by Dolan *et al.* at 61 kbar.<sup>6</sup> Obviously,

the approximate nature of the translation of pressure data to crystal structure data adopted should be born in mind when the pressure shifts are discussed. The *ab initio* embedding model potential which corresponds to the high pressure structure ( $a_0=8.000$  Å) will be referred to as AIEMP(60).

### C. The $\text{CrF}_6^{3-}$ defect cluster

All embedded cluster calculations were performed using the following 146 contracted Gaussian basis functions. For the all-electron chromium atom the  $(14s11p6d3f)$  basis set of Wachters<sup>24</sup> contracted as  $(62111111/4211111/3111/3)$  was used. The fluorines were described using the  $1s$  *ab initio* core model potential of Ref. 15. The corresponding  $(5s/5p)$  valence basis set, augmented by one diffuse  $p$  function (exponent 0.194) optimized in embedded  $\text{F}^-$  calculations, was contracted as  $(41/411)$ . Also, in order to allow for some delocalization of the cluster molecular orbitals which, in addition, enables them to improve the orthogonality against the lattice, a  $(6s/3p)$  completely contracted basis set was included on the closest  $\text{Na}^+$  (100) sites, where the contraction coefficients were taken as the  $2s$  and  $2p$  atomic orbitals of the embedded  $\text{Na}^+$  from the preparatory calculations described above. It should be mentioned that the role of these second-neighbor basis set functions in AIEMP calculations corresponds to that of the inner functions of molecular valence basis sets in molecular core model potential calculations where these functions ensure the proper nodal structure of the valence orbitals. Also, from a detailed test on the performance of second neighbor *ab initio* embedding model potentials compared to all-electron second neighbor cluster calculations in a series of defect crystals ( $\text{Cu}^{2+}$ ,  $\text{Ag}^{2+}\text{:MO}$ ,  $\text{M}=\text{Mg, Ca, Sr}$ )<sup>25</sup> the use of this kind of basis function has proven to be necessary, and to reduce the errors of the AIEMP calculated cluster bond lengths and Jahn–Teller parameters to less than 0.01 Å for the equilibrium distances and less than 5% for the Jahn–Teller energies.

The embedded [either in AIEMP(0) or AIEMP(60)] 69-electron  $\text{CrF}_6^{3-}$  cluster wave functions and energies corresponding to three electronic states ( $^4A_{2g}$  ground state, and  $^4T_{2g}$  and  $^2E_g$  excited states) were optimized along the octahedral totally symmetric stretch coordinate in order to obtain impurity–ligand equilibrium distances and  $a_{1g}$  vibrational frequencies. The optimizations were done at two different levels of accuracy: First, the geometry optimizations were performed through complete active space SCF (CASSCF) calculations<sup>26</sup> including three active electrons in the mainly  $\text{Cr}(3d)$   $t_{2g}$  and  $e_g$  molecular orbitals. These calculations will be referred to as CAS(3). Then, the geometry optimizations were repeated at the three-electron multireference averaged coupled-pair functional (ACPF) level<sup>27,28</sup> based on the CAS(3) configuration space correlating the outermost  $t_{2g}$  and  $e_g$  shells. These calculations will be referred to as ACPF(3). At the CAS(3) and ACPF(3) levels the vibrational frequency corresponding to the  $e_g$  stretching mode was also calculated for the ground state. Finally, at the respective energy minima the vertical absorption and emission transition energies were

calculated by correlating the  $\text{Cr}(3s,3p,3d)$  electrons [ACPF(11)] for the transitions involving the doublet state, while twelve mainly  $\text{F}(2p)$  ( $a_{1g}$ ,  $e_g$ , and  $t_{2g}$ ) and the three  $\text{Cr}(3d)$  electrons were correlated in the ACPF(15) calculations of the quartet–quartet transition energies.<sup>12</sup>

The interaction integrals due to the environment were evaluated using a recently completed one-electron model-potential program which is capable of handling ECP,<sup>29</sup> core AIMP,<sup>15</sup> and environment AIMP<sup>13,14</sup> calculations.<sup>30</sup>

## III. RESULTS AND DISCUSSION

### A. Equilibrium distances and vibrational frequencies

The calculation of the local geometry distortion produced in the perfect  $\text{K}_2\text{NaGaF}_6$  host by the  $\text{Cr}^{3+}$  impurity is considered to be of importance from different points of view: On the one hand, the equilibrium geometries are required for the calculation of other geometry dependent properties following an *ab initio* procedure. On the other hand, from the experimental point of view, the measurement of the local geometry parameters for the ground and excited states of these very diluted materials is very difficult.<sup>31</sup> Under these circumstances, *ab initio* theoretical studies which accurately predict local geometry distortions through the use of quantum mechanical embedding methods could be very valuable. Particularly if, as in the present study, the accurate calculation of the local geometry compression is a key step.

In Table I(A) we have collected the results of the geometry optimizations performed at the CAS(3) and ACPF(3) levels. First of all, the comparison of the calculated ambient pressure equilibrium Cr–F distance  $r_e(\text{Cr–F})=1.91$  Å to the perfect host Ga–F distance ( $x_F=0.235$   $a_0^{21}$ ), 1.940 Å, shows a local distortion where the fluorines come closer by 0.03 Å to the  $\text{Cr}^{3+}$  impurity. The results also show the expected shift to higher  $r_e(\text{Cr–F})$  values of the  $10Dq$  state  $^4T_{2g}$  relative to the bond length of the ground state while the intraconfigurational  $^2E_g$  state is not shifted.

As to the effects of pressure, it can be seen in Table I(A) that all three states show a uniform compression of the bond length by 1.2% to 1.3% (about 0.03 Å). At high pressure, the relative positions of the excited state minima with respect to the ground state minimum show again a shifted  $^4T_{2g}$  state while the  $^2E_g$  state is affected by the same amount as the ground state (see Fig. 1).

Also in Table I(B) and I(C); the calculated and (available) experimental values of the  $a_{1g}$  and  $e_g$  vibrational frequencies are shown. The agreement with the experimental values is very good, with errors always within 2%. The computed pressure induced shifts reproduce the experimental trends reported by Dolan *et al.*<sup>6</sup> quite closely. The value of the ratio of the Grüneisen parameter and bulk modulus,  $\gamma/B$ , estimated by Sliwczuk *et al.*<sup>10</sup> from the pressure dependence of Raman scattering in  $\text{K}_2\text{NaGaF}_6\text{:Cr}^{3+}$  is  $0.0163$   $\text{GPa}^{-1}$  for the  $a_{1g}$  mode. Using the calculated values of the  $a_{1g}$  vibrational frequencies listed in Table I(B), our estimate for the Grüneisen parameter is  $\gamma_{a_{1g}} = 0.910$  which, divided by the estimated iso-

TABLE I. Experimental and calculated values of Cr-F equilibrium distances and vibrational frequencies.

	$^4A_{2g}$			$^4T_{2g}$			$^2E_g$		
	CAS(3)	ACPF(3)	Expt.	CAS(3)	ACPF(3)	Expt.	CAS(3)	ACPF(3)	Expt.
(A) Cr-F equilibrium distances in Å									
0 kbar	1.911	1.911	...	1.943	1.943	...	1.911	1.911	...
61 kbar	1.889	1.889	...	1.918	1.918	...	1.889	1.889	...
% compression	1.2	1.2	...	1.3	1.3	...	1.2	1.2	...
(B) $a_{1g}$ vibrational frequency in $\text{cm}^{-1}$									
0 kbar	582	582	568 <sup>a</sup>	579	579	...	581	582	556 <sup>a</sup>
61 kbar	628	628	630 <sup>b</sup>	630	630	...	628	628	...
% increase	7.9	7.9	10.9	8.8	10.9	...	8.1	7.9	...
(C) $e_g$ vibrational frequency in $\text{cm}^{-1}$									
0 kbar	489	478	481 <sup>c</sup>						
61 kbar	543	543	543 <sup>b</sup>						
% increase	11.0	13.6	12.9						

<sup>a</sup>Reference 1.<sup>b</sup>Reference 6.<sup>c</sup>References 2 and 4.

thermal bulk modulus  $B=51.32 \text{ GPa}^{-1}$  of Sinkovits and Bartran,<sup>11</sup> leads to the computed value for  $\gamma_{a_{1g}}/B = 0.0177 \text{ GPa}^{-1}$ , in good agreement with the value inferred from the Raman scattering experiments.

Finally, it should be noted that the effects of correlating the mainly Cr(3d) electrons [ACPF(3)] is negligible both for the equilibrium geometries and vibrational frequencies as well as for their pressure shifts.

## B. Transition energies

Once the equilibrium geometries and  $a_{1g}$  vibrational frequencies of the  $^4A_{2g}$ ,  $^4T_{2g}$ , and  $^2E_g$  states have been calculated, it is possible to compute the vertical transition energies and correct them, approximately, with the zero point energy. The results of the calculations of the absorption and emission transitions have been collected in Table II. It should be noted that neither distortions to lower than  $O_h$  symmetry nor spin-orbit coupling have been considered; their expected effects on the calculated transitions will be discussed below.

Since the accurate representation of such a subtle differential environmental effect as the pressure induced shifts is a demanding test for any embedding theory, these will be used to evaluate the performance of the present approach. Consequently, we will begin by discussing the calculated vs experimental pressure shifts and then discuss the absolute errors of the calculated transitions, although, owing to their localized nature, they are expected to be more related to differential correlation and other intracluster effects (like vibronic and spin-orbit couplings), than due to the effects of the different environments.

The results in Table II show a blueshift by some  $1100 \text{ cm}^{-1}$  of the quartet-quartet transition energies, both for the  $^4A_{2g} \rightarrow ^4T_{2g}$  absorption and for the  $^4T_{2g} \rightarrow ^4A_{2g}$  emission and no pressure shift in the zero phonon  $^4A_{2g} \leftrightarrow ^2E_g$  transition. All pressure induced shifts appear to be completely independent of the different levels of correlation included in this work, which indicates that the effects of pressure and the correlation effects are not coupled in this system and that the CAS(3) level is an adequate choice.

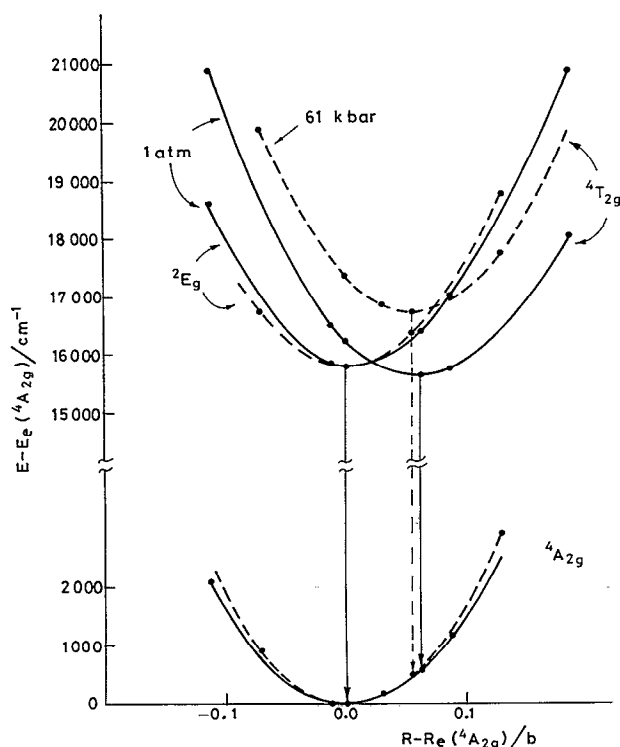


FIG. 1. Ambient pressure (solid lines) and high pressure (dashed lines)  $a_{1g}$  potential energy surfaces of the  $^4A_{2g}$  ground state, and  $^4T_{2g}$  and  $^2E_g$  excited states of  $\text{K}_2\text{NaGaF}_6\text{:Cr}^{3+}$ , corresponding to the *ab initio* embedding model potential calculations. The ACPF(3) potential energy surfaces have been corrected so as to include the calculated ACPF(11) or ACPF(15) correlation corrections to the transition energies plus further atomic ( $-1260 \text{ cm}^{-1}$ ) and molecular [ $-500 \text{ cm}^{-1}$  (Ref. 12)] correlation corrections on the doublet potential energy surface (see the text for details). The ground state  $^4A_{2g}$  equilibrium energies and distances have been arbitrarily set as the origins for the excited state energies and displacements.

TABLE II. Calculated values of the vertical transitions, corrected by the zero point energy, corresponding to the single configuration coordinate ( $a_{1g}$  mode) calculations. All numbers in  $cm^{-1}$ .

	CAS(3)	ACPF(3)	ACPF(15)	Expt.	CAS(3)	ACPF(3)	ACPF(11)	Expt.
(A) Vertical absorptions from the minimum of ${}^4A_{2g}$								
	${}^4A_{2g} \rightarrow {}^4T_{2g}$				${}^4A_{2g} \leftrightarrow {}^2E_g$			
0 kbar	14 540	14 770	15 990	16 150 <sup>a</sup>	19 680	18 730	17 590	15 045(2) <sup>b</sup>
61 kbar	15 590	15 840	17 080	...	19 670	18 720	17 580	15 156(2) <sup>c</sup>
Shift	1 050	1 070	1 090	...	-10	-10	-10	111
(B) Vertical emissions from the minimum of ${}^4T_{2g}$								
	${}^4T_{2g} \rightarrow {}^4A_{2g}$							
0 kbar	13 940	14 170	15 390	13 700(100) <sup>c</sup>				
61 kbar	15 060	15 290	16 550	14 800(100) <sup>c</sup>				
Shift	1 120	1 120	1 160	1 100				

<sup>a</sup>Reference 5.<sup>b</sup>Reference 1.<sup>c</sup>Reference 6.

As to the comparison of the AIEMP results with the experimentally observed shifts, the very good agreement indicates that the pressure-volume relationship assumed here, based on the estimated variation of  $\Delta a_0/a_0$  with pressure from Sinkovits *et al.*<sup>11</sup> is probably accurate. But, more important, from the methodological point of view, it shows the ability of the *ab initio* embedding potentials to accurately reproduce the differential environmental effects caused by hydrostatic pressure. In fact, the interpretation of the strong to weak field pressure-induced transition proposed by Dolan *et al.*<sup>6</sup> is supported by our results: while the  $10Dq$  state is pushed to higher energy values relative to the ground state by the changing *ab initio* embedding model potentials which represent pressure, the intraconfigurational  ${}^2E_g$  remains virtually insensitive to it (Table II, Fig. 1).

One could think, at this stage, that the success in the reproduction of the differential pressure effects lies in the Madelung contribution to the embedding potential. The following results show, however, that the pressure shifts are exclusively due to changing quantum mechanical cluster-lattice interactions. In effect, the comparison of our CAS(3) results to analogous calculations where all the quantum interactions of the embedding potentials are switched off, corresponding to a cluster embedded in a Madelung potential and referred to as PCH, is presented in

Table III. The calculated equilibrium distances and  $a_{1g}$  vibrational frequencies corresponding to a CAS(3) level using either the AIEMP or PCH embedding potentials can be compared. The conclusion is clear. The point charge embedding leads to very loose cluster geometries, low vibrational frequencies (a result also found in other similar defect crystals<sup>13,25</sup>), and a *null* effect of pressure. Therefore, the correct trends shown by the AIEMP results are directly ascribable to interactions beyond the point-charge level, that is, cluster-lattice short-range Coulomb, exchange, and orthogonality. The same is true for the transition energies which show negligible shifts with the changing lattice volume when only the Madelung part is included:  ${}^4A_{2g} \rightarrow {}^4T_{2g} = 12\,600\,cm^{-1}$ ,  ${}^4A_{2g} \leftrightarrow {}^2E_g = 19\,700\,cm^{-1}$ ,  ${}^4T_{2g} \rightarrow {}^4A_{2g} = 11\,000\,cm^{-1}$ , with shifts by  $-20$ ,  $+6$ , and  $100\,cm^{-1}$ , respectively.

Finally, once the differential effects of pressure have been presented, we can discuss the absolute errors of the computed transition energies. First of all, it can be seen in Table II that the improvements introduced by correlating more than three electrons are very similar to those found by Pierloot and Vanquickenborne<sup>12</sup> in their calculations on isolated  $CrF_6^{3-}$ . The transitions to the  ${}^2E_g$  state are lowered by some  $1100\,cm^{-1}$  (compared to the  $1500\,cm^{-1}$  correction from Ref. 12) as the Cr 3s and 3p electrons are also correlated. The calculated transition energies to or from

TABLE III. Experimental and calculated [CAS(3)] values of Cr-F equilibrium distances and vibrational frequencies corresponding to the *ab initio* embedding model potential (AIEMP) and to the Madelung embedding potential (PCH).

	${}^4A_{2g}$			${}^4T_{2g}$			${}^2E_g$		
	AIEMP	PCH	Expt.	AIEMP	PCH	Expt.	AIEMP	PCH	Expt.
(A) Cr-F equilibrium distances in Å									
0 kbar	1.911	1.961	...	1.943	2.006	...	1.911	1.963	...
61 kbar	1.889	1.962	...	1.918	2.006	...	1.889	1.964	...
(B) $a_{1g}$ vibrational frequency in $cm^{-1}$									
0 kbar	582	473	568 <sup>a</sup>	579	451	...	581	472	556 <sup>a</sup>
61 kbar	628	471	630 <sup>b</sup>	630	465	...	628	462	...

<sup>a</sup>Reference 1.<sup>b</sup>Reference 6.

the  ${}^4T_{2g}$  state are increased by about  $1200\text{ cm}^{-1}$  [compared to  $1000\text{ cm}^{-1}$  (Ref. 12)], as the additional 12 electrons in the  $a_{1g}$ ,  $e_g$ , and  $t_{2g}$   $F(2p)$  orbitals are also correlated. When these higher-level results are compared to the available experimental data, it can be seen that the absorption to the  ${}^4T_{2g}$  state is obtained very close to the experimental value (in error by some  $-160\text{ cm}^{-1}$ ). The emissions from the  ${}^4T_{2g}$  are calculated some  $1700\text{ cm}^{-1}$  too high, and the zero-phonon  ${}^4A_{2g} \leftrightarrow {}^2E_g$  transitions are calculated about  $2500\text{ cm}^{-1}$  above the experimental values. If we now consider, for the transitions to the doublet, the atomic error due to the truncation of the Cr one-electron and many-electron basis sets, which can be estimated as some  $1260\text{ cm}^{-1}$ ,<sup>32</sup> and the expected  $400\text{--}600\text{ cm}^{-1}$  further correction that a combined 25 electron correlation treatment would bring,<sup>12</sup> the  $2500\text{ cm}^{-1}$  discrepancy would be reduced to some  $600\text{--}800\text{ cm}^{-1}$ . (The so corrected potential energy surfaces are shown in Fig. 1.) This residual discrepancy, as well as the  $1700\text{ cm}^{-1}$  error of the  ${}^4T_{2g} \rightarrow {}^4A_{2g}$  emission, are consistent with the intracluster vibronic couplings in the excited states and their interplay with the spin-orbit coupling which have not been included in the present work. In fact, if as expected, the  ${}^4T_{2g}$  excited state undergoes a Jahn-Teller distortion out of its  $a_{1g}$  minimum, the absolute values of the emission calculated from the new (distorted) equilibrium configuration would be considerably lowered. Furthermore, also the possibility of a second-order Jahn-Teller effect on the  ${}^2E_g$  state has been pointed out by Flint.<sup>2</sup> The calculation of the Jahn-Teller energy surfaces of the excited states is beyond the scope of this work, however, and will be the subject of forthcoming work.

#### IV. CONCLUSIONS

In this paper we present the results of an *ab initio* study of the pressure effects of the  ${}^4A_{2g}$  ground state and the  ${}^4T_{2g}$  and  ${}^2E_g$  excited states of  $\text{Cr}^{3+}$ -doped  $\text{K}_2\text{NaGaF}_6$ .

CASSCF and ACPF calculations on the  ${}^4A_{2g}$  ground state and the  ${}^4T_{2g}$  and  ${}^2E_g$  excited states of a  $\text{CrF}_6^{3-}$  cluster embedded in an AIMP representation of the  $\text{K}_2\text{NaGaF}_6$  lattice at ambient pressure and 61 kbar have been performed. The calculated pressure shifts on electronic transitions and vibrational frequencies are in close agreement with available experimental results on  $\text{Cr}^{3+}$ -doped  $\text{K}_2\text{NaGaF}_6$ . Thus the *ab initio* embedding model potential method provides a reliable tool to accurately model hydrostatic pressure experiments in this type of defect crystals. The analysis of the results shows that the subtle differential environmental effects brought about by pressure are due to the part of the embedding potential that represents deviations from the Madelung contribution. The point-charge representation of the crystalline lattice leads to too long internal cluster distances, too low vibrational frequencies, and a zero effect of pressure.

#### ACKNOWLEDGMENTS

This work was partly supported by funds from the Swedish Consortium on Oxidic Overlayers and by a grant from MEC (DGICYT PS89-0021), Spain.

- <sup>1</sup>J. Ferguson, H. J. Guggenheim, and D. L. Wood, *J. Chem. Phys.* **54**, 504, (1971).
- <sup>2</sup>C. D. Flint, *Chem. Phys. Lett.* **11**, 27 (1971).
- <sup>3</sup>K. Y. Wong, N. B. Manson, and G. A. Osborne, *J. Phys. Chem. Solids* **38**, 1017 (1977).
- <sup>4</sup>P. Greenough and G. Paulusz, *J. Chem. Phys.* **70**, 1967 (1979).
- <sup>5</sup>L. Dubicki, J. Ferguson, and B. van Oosterhout, *J. Phys. C* **13**, 2791 (1980).
- <sup>6</sup>J. F. Dolan, L. A. Kappers, and R. H. Bartram, *Phys. Rev. B* **33**, 7339 (1986).
- <sup>7</sup>L. J. Andrews, A. Lempicki, B. C. McCollum, C. J. Giunta, R. H. Bartram, and J. F. Dolan, *Phys. Rev. B* **34**, 2735 (1986).
- <sup>8</sup>R. H. Bartram, J. C. Charpie, L. J. Andrews, and A. Lempicki, *Phys. Rev. B* **34**, 2741 (1986).
- <sup>9</sup>U. Sliwczuk, R. H. Bartram, D. R. Gabbe, and B. C. McCollum, *J. Phys. Chem. Solids* **52**, 357 (1991).
- <sup>10</sup>U. Sliwczuk, A. G. Rinzler, L. A. Kappers, and R. H. Bartram, *J. Phys. Chem. Solids* **52**, 363 (1991).
- <sup>11</sup>R. S. Sinkovits and R. H. Bartram, *J. Phys. Chem. Solids* **52**, 1137 (1991).
- <sup>12</sup>K. Pierloot and L. G. Vanquickenborne, *J. Chem. Phys.* **93**, 4154 (1990).
- <sup>13</sup>Z. Barandiarán and L. Seijo, *J. Chem. Phys.* **89**, 5739 (1988).
- <sup>14</sup>Z. Barandiarán and L. Seijo, in *Computational Chemistry: Structure, Interactions and Reactivity*, edited by S. Fraga, Studies in Physical and Theoretical Chemistry, Vol. 77(B) (Elsevier, Amsterdam, 1992), pp. 435-461.
- <sup>15</sup>S. Huzinaga, L. Seijo, Z. Barandiarán, and M. Klobukowski, *J. Chem. Phys.* **86**, 2132 (1987); L. Seijo, Z. Barandiarán, and S. Huzinaga, *ibid.* **91**, 7011 (1989); Z. Barandiarán, L. Seijo, and S. Huzinaga, *ibid.* **94**, 3762 (1991).
- <sup>16</sup>R. McWeeny, *Proc. R. Soc. London, Ser. A* **253**, 242 (1959); *Rev. Mod. Phys.* **32**, 335 (1960); M. Kleiner and R. McWeeny, *Chem. Phys. Lett.* **19**, 476 (1973); R. McWeeny, *Methods of Molecular Quantum Mechanics* (Academic, London, 1989).
- <sup>17</sup>S. Huzinaga and A. A. Cantu, *J. Chem. Phys.* **55**, 5543 (1971); S. Huzinaga, D. McWilliams, and A. A. Cantu, *Adv. Quantum Chem.* **7**, 187 (1973).
- <sup>18</sup>Z. Barandiarán and L. Seijo, in *Cluster Models for Surface and Bulk Phenomena*, Proceedings of the NATO ARW, Erice, Sicily, 1991, edited by G. Pacchioni and P. Bagus (Plenum, New York, 1992).
- <sup>19</sup>W. H. Adams, *J. Chem. Phys.* **34**, 89 (1961).
- <sup>20</sup>K. Knox and D. W. Mitchell, *Inorg. Nucl. Chem.* **21**, 253 (1961).
- <sup>21</sup>B. Boulard and C. Jacoboni, *J. Solid State Chem.* **80**, 17 (1989).
- <sup>22</sup>H. M. Evjen, *Phys. Rev.* **39**, 675 (1932).
- <sup>23</sup>Note that the host crystal structure, a periodic nonlocal property, is always taken from the experimental data in the AIMP approach. For these data to be taken from *ab initio* periodic calculations, a similar level as that used for the defect cluster, that is, including correlation effects beyond Hartree-Fock, would have to be considered.
- <sup>24</sup>A. J. H. Wachters, *J. Chem. Phys.* **52**, 1033 (1970).
- <sup>25</sup>J. L. Pascual, L. Seijo, and Z. Barandiarán (to be published).
- <sup>26</sup>B. O. Roos, P. R. Taylor, and P. E. M. Siegbahn, *Chem. Phys. Lett.* **48**, 157 (1980).
- <sup>27</sup>R. Ahlrichs, P. Scharf, and C. Ehrhardt, *J. Chem. Phys.* **82**, 890 (1985).
- <sup>28</sup>R. J. Gdanitz and R. Ahlrichs, *Chem. Phys. Lett.* **143**, 413 (1988).
- <sup>29</sup>L. G. M. Pettersson, U. Wahlgren, O. Gropen, *J. Chem. Phys.* **86**, 2176 (1987).
- <sup>30</sup>ECPAIMP is an integral program for ECP and AIMP calculations written by L. G. M. Pettersson and L. Seijo.
- <sup>31</sup>*EXAFS Spectroscopy. Technique and Applications*, edited by B. K. Teo and D. C. Joy (Plenum, New York, 1981).
- <sup>32</sup>The free  $\text{Cr}^{3+}$  transition  ${}^4F \rightarrow {}^2G$  is calculated to be  $15\,960\text{ cm}^{-1}$  at the ACPF(11) level, which compared to the (average over different  $J$  levels) experimental value  $14\,699\text{ cm}^{-1}$  (Ref. 33) leads to an atomic error of about  $1260\text{ cm}^{-1}$  which is expected to be transferred to the cluster  ${}^4A_{2g} \rightarrow {}^2E_g$  transition (Ref. 34).
- <sup>33</sup>J. Sugar and C. Corliss, *J. Phys. Chem. Ref. Data* **6**, 317 (1977).
- <sup>34</sup>L. Pueyo and J. W. Richardson, *J. Chem. Phys.* **67**, 3583 (1977).